

## Collective Rearrangement at the Onset of Flow of a Polycrystalline Hexagonal Columnar Phase

Teresa Bauer, Julian Oberdisse, and Laurence Ramos\*

Laboratoire des Colloïdes, Verres et Nanomatériaux (UMR CNRS-UM2 5587), CC26, Université Montpellier 2,  
34095 Montpellier Cedex 5, France

(Received 24 July 2006; published 21 December 2006)

Creep experiments on polycrystalline surfactant hexagonal columnar phases show a power law regime, followed by a drastic fluidization before reaching a final stationary flow. The scaling of the fluidization time with the shear modulus of the sample and stress applied suggests that the onset of flow involves a bulk reorganization of the material. This is confirmed by x-ray scattering under stress coupled to *in situ* rheology experiments, which show a collective reorientation of all crystallites at the onset of flow. The analogy with the fracture of heterogeneous materials is discussed.

DOI: 10.1103/PhysRevLett.97.258303

PACS numbers: 82.70.-y, 83.50.-v

Yield stress fluids are materials that respond elastically below a yield stress,  $\sigma_y$ , and flow as liquids for stresses above  $\sigma_y$  [1]. Typical materials that fall into this category include granular media, dry foams, or dense colloidal suspensions and emulsions. Very recently, Bécu *et al.* [2] have shown that the behavior of concentrated emulsions at the onset of flow depends crucially on the microscopic interactions between the droplets, thus underlining the nonuniversal nature of the solid to fluid transition of yield stress fluids. Several fundamental issues are still unclear regarding this transition. These include, in particular, the possible prediction of if and when a material will flow, from its behavior prior to flow. In addition, whether the solid to fluid transition is accompanied by structural modifications of the yield stress fluids remains largely unknown.

We perform creep experiments in order to investigate the onset of flow of soft polycrystalline hexagonal columnar phases. Upon application of a small and constant stress,  $\sigma$ , the material deforms plastically in a similar manner as a solid [3]. By contrast, under high stress, it behaves as a fluid and flows with a constant shear rate that depends on  $\sigma$  [4,5]. Quite remarkably, for an intermediate value of  $\sigma$ , an intriguing regime is observed during which the material, after an incubation time that depends on both  $\sigma$  and the sample shear modulus, evolves suddenly from a power law creep to a flow regime, through a dramatic decrease of the viscosity. Thanks to a combination of synchrotron x-ray scattering experiments under stress and *in situ* rheology measurements, we are able to correlate the solid to fluid transition with structural modifications of the material, thus shedding light on the mechanisms involved at the onset of flow of some complex fluids.

The experimental system is a lyotropic hexagonal phase consisting of infinitely long oil tubes which are stabilized by a surfactant monolayer and immersed in water. The tubes of uniform radius arrange on a triangular array and therefore form a two-dimensional columnar crystal. The samples' composition and elasticity have been described elsewhere [3,6]. Four samples with variable shear moduli,  $G_0$ , ranging from 250 to 3200 Pa, have been investigated.

Rheology experiments are performed on a stress-controlled Paar Physica UDS 200 rheometer in a Couette geometry with a gap of 1 mm. Once loaded in the cell, the sample is systematically cooled below the hexagonal to isotropic fluid phase transition temperature ( $\sim 10^\circ\text{C}$ ), and then warmed up to room temperature. A polycrystal, with an isotropic distribution for the crystallites orientation, is thus rapidly recovered. At time  $t = 0$ , we then apply a constant shear stress,  $\sigma$ , to the material and record the time evolution of the strain,  $\gamma$ . An instantaneous jump of  $\gamma$  is measured, revealing the elastic nature of the material at high frequency, which is followed by a monotonic increase of  $\gamma$ . The evolution of the instantaneous shear rate,  $\dot{\gamma}$ , calculated as the time derivative of  $\gamma$ , is shown in Fig. 1 for several stresses, and displays three distinct regimes. Initially,  $\dot{\gamma}$  decreases as a power law with time, indicating a continuous increase of the instantaneous viscosity,  $\eta$ , defined as  $\sigma/\dot{\gamma}$ . This power law regime is followed by a very abrupt increase of  $\dot{\gamma}$  of more than 2 orders of magnitude, until the shear rate reaches a constant and high value, which corresponds to a stationary flow with a lower viscosity. For  $t$  larger than 0.1 s (the time resolution of our experiments), and over at least 3 orders of magnitude, we find in the

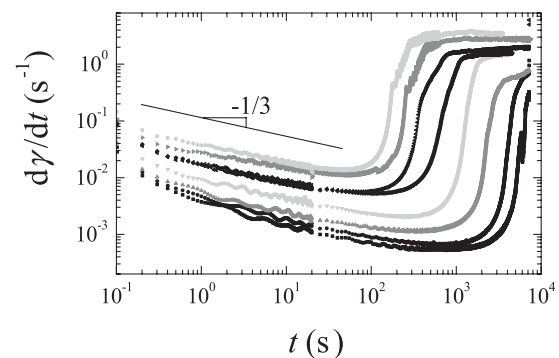


FIG. 1. Time evolution of the shear rate in creep experiments for a sample with an elastic shear modulus  $G_0 = 2240$  Pa. At time 0 a constant stress  $\sigma = 12, 13, 15, 19, 21, 22, 30, 35$  Pa (from bottom to top) is applied to the sample.

power law regime  $\dot{\gamma} \sim t^p$  with  $p = -0.34 \pm 0.05$ , whatever  $\sigma$  and  $G_0$ . This regime recalls the primary creep regime, the so-called Andrade creep [7] measured in many crystalline and noncrystalline materials. However, the catastrophic acceleration of the shear rate that follows the primary creep, which illustrates a drastic decrease of the viscosity, is neither observed for metallic materials nor for yield stress fluids such as foams [8] or colloidal glasses [9], where the transition from creep to flow is smooth. The features shown in Fig. 1 appear rather unique for a complex fluid, but in fact display intriguing analogies with the fracture under constant load of many composite heterogeneous materials [10,11]. We define the fluidization time,  $\tau_f$ , as the time at which  $\dot{\gamma}$  is minimum (i.e., the instantaneous viscosity is maximum).

We report the stress dependence of the fluidization time in Fig. 2(a), for several samples with different elasticities. We find that, for all samples,  $\tau_f$  decreases as  $\sigma$  increases, and that curves for softer samples are shifted to lower stresses. Interestingly, all data points can be put onto a single master curve if the stress is renormalized by a power law of the shear modulus,  $G_0^m$ . We find the best collapse of the data for  $m = 0.64$ . For this value, the master curve can be reasonably well fitted with a power law  $\tau_f \sim (\sigma/G_0^{0.64})^{(-3.1 \pm 0.2)}$  [Fig. 2(b)]. This scaling implies that there is no divergence of  $\tau_f$  with stress. It indicates that the material does not show any detectable yield stress in our experimental time window, in contrast with the findings for micellar polycrystals for instance [12]. On the other hand, we have shown previously that the shear modulus of the polycrystal scales as  $R^{-3}$ , where  $R$  is the radius of the surfactant tubes [3]. Hence, the normalized stress  $\sigma/G_0^{0.64}$  scales roughly as  $\sigma \times R^2$ . We expect the number density of tubes in the material to scale as  $1/R^2$ . Thus, the master curve indicates that  $\tau_f$  depends only on the stress applied per tube. Interestingly, despite variation

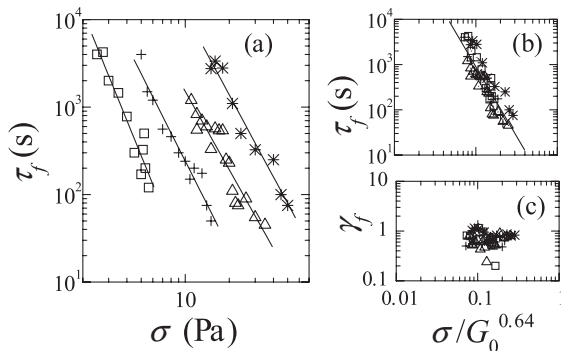


FIG. 2. Fluidization time,  $\tau_f$ , as a function of (a) the stress applied  $\sigma$ , and (b)  $\sigma/G_0^{0.64}$  (symbols), for samples with different shear moduli,  $G_0 = 250$  Pa (squares),  $760$  Pa (crosses),  $2240$  Pa (triangles), and  $3200$  Pa (stars); the line in (b) is a power law fit yielding an exponent  $-3.1 \pm 0.2$ . (c) Strain at  $t = \tau_f$  as a function of  $\sigma/G_0^{0.64}$  [same symbols as in (a),(b)].

of  $\tau_f$  of 2 orders of magnitude, the strain  $\gamma_f$  at time  $t = \tau_f$  is approximately constant. We find  $\gamma_f \approx (69 \pm 23)\%$ , irrespective of the stress applied and of the sample elasticity [Fig. 2(c)]. This shows that the onset of flow results from a strain controlled mechanism. Note that a critical strain similar to ours (i.e., of the order of 1) is typical for shear-induced order in hard sphere suspensions [13] or to completely fluidize a foam sample. Both a critical strain of 1 and the remarkable dependence of the stress with the number of tube suggest that the fluidization time reflects a bulk mechanism that involves the whole sample and not an interfacial property. This is supported by the results described below.

In order to gain a better understanding of the mechanisms at work in the creep regime and at the onset of flow, we have coupled time-resolved Synchrotron small-angle x-ray scattering (SAXS) under stress to *in situ* rheological measurements. Experiments have been performed on the ID-2 beam line at the ESRF, Grenoble, France. A stress-controlled Haake RS300 rheometer equipped with a Couette cell is used. The scattering profiles are recorded for two geometries, the incident beam being either radial or tangential with respect to the cell. Only the softer sample ( $G_0 = 250$  Pa) has been investigated. A procedure analogous to the one used for the rheology experiments has been performed in order to ensure a reproducible polycrystalline initial state corresponding to an isotropic distribution for the orientation of the crystallites, as confirmed by isotropic rings found in the SAXS patterns for both radial and tangential geometries. We can evaluate that the size of the crystallites is of the order of  $1 \mu\text{m}$  [14]. Taking into account the size of the incident beam ( $100 \mu\text{m}$ ) and that of the gap ( $1 \text{ mm}$ ), we conclude that the SAXS spectra reflects the orientation distribution of a large assembly of crystallites.

A typical series of radial scattering patterns are shown in Fig. 3(a) together with the strain,  $\gamma$ , and the instantaneous viscosity,  $\eta$ . The time evolution of  $\eta$  clearly shows the three successive regimes (power law creep, fluidization, and stationary flow) described previously. In Fig. 3(a), the time is normalized by  $t_c$ , the time at which the material starts to flow with a stationary shear rate. The SAXS patterns exhibit isotropic rings at the beginning of the experiment, and then convert into a markedly anisotropic signal in the flow regime, with higher intensity along the vorticity direction ( $\theta = 90^\circ$  and  $270^\circ$ ). To quantify the time evolution of the patterns and correlate it with that of the rheological properties, we compute the angular dependence of the scattered intensity integrated around the first Bragg peak (azimuthal scan), and identify the angular position of the local maxima. Figure 3(b) displays the evolution of the position and intensity of these maxima, for  $\theta$  in the range  $160^\circ - 340^\circ$  ( $\theta = 0^\circ$  and  $180^\circ$  corresponds to the velocity direction). The experimental data clearly show that, as soon as the systems flows ( $t/t_c \geq 1$ ),

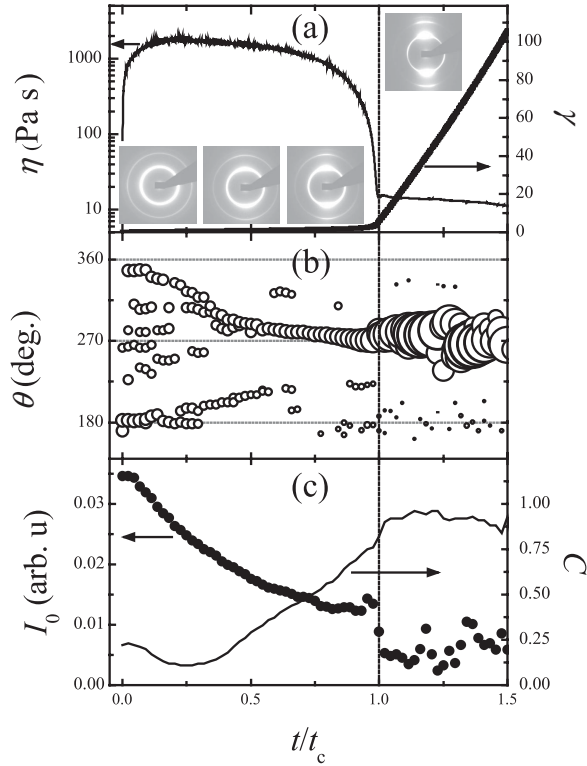


FIG. 3. Combined rheological and structural measurements in a creep experiment. The sample elasticity is  $G_0 = 250$  Pa and the stress is  $\sigma = 2$  Pa. The time is normalized by the time  $t_c$  at which the sample flows with a constant shear rate. The dashed vertical line marks the beginning of a stationary flow regime. (a) *In situ* rheological measurements, strain (thick line) and instantaneous viscosity (thin line), and SAXS patterns taken from left to right at  $t/t_c = 0.25, 0.75, 0.98$ , and  $1.14$ . The gray scale is linear and identical for all images. (b) Time evolution of the angular position of the local intensity maxima in an azimuthal scan. The bubble size scales with intensity. (c) Time evolution of the contrast  $C$  (line) and the scattered intensity at  $\theta = (180 \pm 2)^\circ$  (solid circles).

the surfactant tubes are in majority aligned along the flow (maxima around  $270^\circ$ ), although the angular distribution for the tubes orientation is wide ( $\Delta\theta \sim 35^\circ$ ). We note that the angular width,  $\Delta\theta$ , and the shear rate measured in the flow regime ( $\dot{\gamma} = 0.14 \text{ s}^{-1}$  for  $\sigma = 2$  Pa) are in quantitative agreement with our previous findings [4,5] concerning both the continuous decrease of  $\Delta\theta$  as  $\dot{\gamma}$  increases and the stress dependence of  $\dot{\gamma}$ , suggesting that the flow regime investigated here belongs to the shear-thinning regime previously determined for  $\dot{\gamma}$  in the range  $(1\text{--}40) \text{ s}^{-1}$ . We calculate the contrast,  $C$ , defined as  $(I_{\max} - I_{\min}) / (I_{\max} + I_{\min})$ , where  $I_{\max}$  and  $I_{\min}$  are, respectively, the maximal and minimal intensity along the azimuthal scan profile;  $C$  varies between 0 (for a perfectly isotropic distribution of the crystallite orientation) and 1 (for a totally anisotropic distribution). As shown in Fig. 3(c),  $C$  is small ( $\approx 0.25$ ) at the beginning of the experiment, and after a slight decrease

[15], increases continuously, until it reaches a constant and high value,  $C \approx 0.92$ , at  $t = t_c$ .

Because each experiment probes a given ensemble of crystallites, the exact patterns of the peak position along a scan change from one experiment to another one; in particular, the intensity around  $\theta = 90^\circ$  and  $270^\circ$  does not exhibit a clear trend in the power law creep regime. Two experimental observations are nevertheless robust. The first one is the systematic concomitance of the contrast  $C$  reaching its plateau value with the onset of flow. This findings demonstrate that the onset of flow is characterized by a collective rearrangement of all crystallites such that they all orient along the flow direction, hence the flow is homogeneous, rather than by wall slippage (as observed in the vicinity of the yield stress for a microgel paste [16]), or shear localization (as observed in adhesive emulsions [2] or wet granular media [17]). Moreover, this mechanism is in agreement with the rheology experiments (Fig. 2) which indicate a bulk mechanism. Note in addition that data recorded in tangential geometry do not show any significant variation with time: isotropic rings are always measured, showing that, in the direction perpendicular to the flow, the sample texture remains powderlike, and the width of the Bragg peaks do not vary, indicating a fixed average crystallites size. These observations are consistent with the physical picture that only the orientation of crystallites changes in the creep and at the onset of flow. This also compares favorably with simulations of polycrystals that show rotation of individual grains under a constant external load [18].

The second robust experimental observation concerns  $I_0$ , the scattered intensity for  $\theta = (180 \pm 2)^\circ$ .  $I_0$  arises from the scattering of tubes that are perpendicular to the flow (tubes parallel to both the vorticity direction and the velocity gradient direction contribute to  $I_0$ ), and resist flow. As shown in Fig. 3(c),  $I_0$  decreases continuously with time and drops down to a smaller and constant value once the

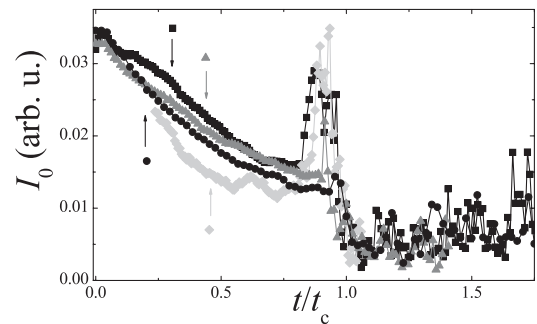


FIG. 4. Scattered intensity in the direction perpendicular to the flow [ $\theta = (180 \pm 2)^\circ$ ] for four distinct experiments, with applied stress of 2 (circles and up-pointing triangles), 2.5 (squares), and 3 Pa (diamonds). The time is normalized by the time  $t_c$  at which the sample flows, and the intensity by the scattered intensity integrated over all angles in the flow regime. The arrows indicate the normalized fluidization time,  $\tau_f/t_c$ .

sample flows. Similar features are systematically measured, as shown in Fig. 4, where the time evolution of  $I_0$  for several experiments is reported. In Fig. 4, time is normalized by  $t_c$ , and the absolute scattered intensity by  $I$ , the intensity integrated over all angles in the flow regime [19]. We note that not only the time evolution but also the absolute value of  $I_0$  are very similar for all experiments, which suggests that the evolution of  $I_0$  reflects a very general mechanism. A peak of  $I_0$  is nevertheless sometimes observed, just before the collective reorientation of all crystallites (at  $t = t_c$ ) and well after the fluidization time. It is presumably due to a transient orientation of some crystallites (with tubes perpendicular to the flow) required to reach a more favorable orientation as the stationary flow begins.

As pointed out above, the whole time evolution of the shear rate (Fig. 1) presents strong analogies with the strain rate time evolution measured in the extension creep of composite heterogeneous materials except that, in our case, the acceleration of the rate (fluidization regime) is followed by a stationary flow with low viscosity. By contrast, in extension creep of heterogeneous materials, it is followed by the fracture of the sample [10,11]. Based on this analogy, we propose a phenomenological picture for our experimental observations, which is inspired by the fiber bundle models [20], and which explains the time evolution of both  $I_0$  and the shear rate  $\dot{\gamma}$ . The initial state of our material is powderlike, with a random and isotropic orientation of the crystallites. We assume that “perpendicular crystallites,” i.e., crystallites for which the tubes are perpendicular to the flow direction (those which contribute to  $I_0$ ), form some sort of percolated network which resists flow. Upon application of a stress, these crystallites progressively reorient, hence  $I_0$  decreases, starting from the easiest ones (the reorientation being more or less easy, based presumably on the local configuration with the neighboring crystallites). Thus, we expect  $\dot{\gamma}$  to decrease as the rate of reorientation decreases, until the network formed by these crystallites is not percolated anymore. This would sign the onset of the fluidization regime, where  $\dot{\gamma}$  increases and facilitates the reorientation of the remaining perpendicular crystallites; hence,  $I_0$  continues to decrease. Once all perpendicular crystallites are reoriented,  $I_0$  reaches a constant minimum value and the sample is expected to flow with a constant  $\dot{\gamma}$ . To reinforce the analogy between creep fracture and onset of flow, experiments with a sufficient temporal and spatial resolution would be required in order to determine the distribution of waiting times between reorientation events and compare it with the power law distributions measured in creep fracture [11,21].

We thank L. Cipelletti, V. Trappe, and L. Vanel for discussions, G. Porte for a critical reading of the manu-

script, and E. Di Cola and P. Panine for technical assistance during the SAXS experiments. T.B. acknowledges partial support from the French-German Collaborative Research Group “Complex Fluids: from 2 to 3 Dimensions,” jointly funded by the DFG (Germany), and the CEA and CNRS (France). This work was supported in part by the NOE “SoftComp” (NMP3-CT-2004-502235) and by the ESRF.

---

\*Electronic address: ramos@lcvn.univ-montp2.fr

- [1] H. A. Barnes, *J. Non-Newtonian Fluid Mech.* **81**, 133 (1999).
- [2] L. Bécu, S. Manneville, and A. Colin, *Phys. Rev. Lett.* **96**, 138302 (2006).
- [3] L. Ramos and F. Molino, *Europhys. Lett.* **51**, 320 (2000).
- [4] L. Ramos, F. Molino, and G. Porte, *Langmuir* **16**, 5846 (2000).
- [5] L. Ramos and F. Molino, *Phys. Rev. Lett.* **92**, 018301 (2004).
- [6] L. Ramos and P. Fabre, *Langmuir* **13**, 682 (1997).
- [7] E. N. da C. Andrade, *Proc. R. Soc. A* **84**, 1 (1910); **90**, 329 (1914); M.-C. Miguel *et al.*, *Phys. Rev. Lett.* **89**, 165501 (2002).
- [8] S. Cohen-Addad, R. Höhler, and Y. Khidas, *Phys. Rev. Lett.* **93**, 028302 (2004).
- [9] G. Petekidis, D. Vlassopoulos, and P.N. Pusey, *J. Phys. Condens. Matter* **16**, S3955 (2004).
- [10] H. Nechad *et al.*, *Phys. Rev. Lett.* **94**, 045501 (2005).
- [11] A. Guarino *et al.*, *Eur. Phys. J. B* **26**, 141 (2002).
- [12] E. Eiser, F. Molino, and G. Porte, *Eur. Phys. J. E* **2**, 39 (2000).
- [13] B.J. Ackerson and P.N. Pusey, *Phys. Rev. Lett.* **61**, 1033 (1988).
- [14] The standard Laue-Scherrer relation relates the width of the Bragg peaks,  $\Delta q$ , to a translational correlation length,  $\xi$ , which can be approximated as the average size of the crystallites:  $\xi \approx 2\pi/\Delta q$ . The full width at half maximum of the first order diffraction peak is of the order of  $8 \times 10^{-3} \text{ nm}^{-1}$  (with a resolution of  $3 \times 10^{-3} \text{ nm}^{-1}$ ); hence  $\xi \approx 1.3 \text{ }\mu\text{m}$ .
- [15] The initial behavior of  $C$  changes from one experiment to another one, and presumably depends on the precise distribution of orientation for the crystallites.
- [16] S.P. Meeker, R.T. Bonnecaze, and M. Cloitre, *Phys. Rev. Lett.* **92**, 198302 (2004).
- [17] N. Huang *et al.*, *Phys. Rev. Lett.* **94**, 028301 (2005).
- [18] R. Ahluwalia, T. Lookman, and A. Saxena, *Phys. Rev. Lett.* **91**, 055501 (2003).
- [19] Note that in the flow regime  $I$  is largely dominated by the intensity at  $\theta = 90^\circ$  and  $270^\circ$ .
- [20] *Statistical Models for the Fracture of Disordered Media*, edited by H.J. Herrmann and S. Roux (Elsevier, Amsterdam, 1990).
- [21] F. Kun *et al.*, *Europhys. Lett.* **63**, 347 (2003).